Materials and Interfaces

A non-swelling silica–poly(acrylic acid) composite for efficient and simultaneous removal of cationic dye, heavy metal and surfactant-stabilized emulsion from wastewater

Yuling Tang, Yuqi Li, Yingjiao Zhang, Chuanhui Mu, Jianfei Zhou, Wenhua Zhang, and Bi Shi

Ind. Eng. Chem. Res., **Just Accepted Manuscript** • DOI: 10.1021/acs.iecr.9b05120 • Publication Date (Web): 31 Jan 2020

A non-swelling silica–poly(acrylic acid) composite for efficient and simultaneous removal of cationic dye, heavy metal and surfactant-stabilized emulsion from wastewater

Yuling Tang,† Yuqi Li,† Yingjiao Zhang,† Chuanhui Mu,† Jianfei Zhou,*,† Wenhua Zhang,† and Bi Shi†,‡

† National Engineering Laboratory for Clean Technology of Leather Manufacture, Sichuan University, Chengdu 610065, PR China

‡ Key Laboratory of Leather Chemistry and Engineering (Sichuan University), Ministry of Education, Chengdu 610065, PR China

ABSTRACT: The discharge of emulsion, cationic dyes, and heavy metals often coexist in wastewaters, greatly enhancing the difficulty of processing. In this work, we fabricated a non-swelling silica–poly(acrylic acid) (SiO_2-PAA) composite through the surface modification of SiO_2 using poly(acrylic acid) (PAA) to remove emulsion, cationic dyes, and heavy metal co-contaminants simultaneously. In SiO_2-PAA composite, PAA exists in a linear and divergent form rather than a network structure. Thus, SiO_2-PAA can gain non-swelling property and provide abundant carboxyl groups as the binding sites for pollutant removal, which is an important advance of PAA based material and improve the potential of practical application. The characterization results of SiO_2-PAA demonstrated PAA was successfully grafted on SiO_2. In a monocomponent system, SiO_2-PAA exhibited excellent separation efficiency for cetyltrimethyl ammonium bromide (CTAB)-stabilized emulsion separation and admirable adsorption capacity of 758.6 and 178.6 mg/g for methylene blue (MB) and Cr(III). This finding was ascribed to the exposure of carboxyl groups in SiO_2-PAA, which could increase the mass transfer efficiency. Importantly, the SiO_2-PAA composite exhibited high efficiency in the simultaneous uptake of CTAB-stabilized emulsion, MB, and Cr(III) co-contaminants. Thus, given the simple fabrication, efficient emulsion separation, admirable adsorption capacity, and excellent reusability of SiO_2-PAA, it exhibits striking potential for the efficient treatment of coexisting pollutants.

KEYWORDS: Silica-poly(acrylic acid), surfactant-stabilized emulsions separation, Cr(III), cationic dyes, adsorption

1. INTRODUCTION

In recent years, rapid industrial development has resulted in large amounts of wastewater with complex components.[1] Surfactant-stabilized emulsions, cationic dyes, and heavy metals usually coexist in wastewater, especially effluents of dye-manufacturing, textile industries and leather making, thereby resulting in the stable existence of pollutants and enhancing the difficulty of treatment.[2-4] Many of these pollutants are non-biodegradable and can affect ecosystems and human health. Significant efforts have been made to remove a single class of pollutant from water systems (emulsion, cationic dyes, or heavy metals).[5-7] However, the treatment of emulsion, cationic dyes, and heavy metal co-contaminated water is still challenging due to their different physicochemical characteristics. Therefore, designing and manufacturing novel multifunctional materials to purify wastewater containing emulsion, cationic dyes, and heavy metal ions are still crucial.

Poly(acrylic acid) (PAA), a water-soluble linear polymer that contains abundant carboxyl groups, has gained significant attention in environmental processes.[8-9] The most important feature of PAA is that the abundant carboxyl groups exhibit strong ability to combine with heavy metal ions and cationic dyes and can make the emulsion unstable.[10-12] However, the water-soluble property of linear PAA hinders its direct application to purify wastewater. Therefore, the synthesis of water-insoluble PAA hydrogels with three-dimensional net structure has attracted considerable attention.[13] Huang et al. synthesized P(AMPS-co-AA) hydrogel using acrylic acid and 2-acrylamido-2-methyl-propanesulfonic acid for the extraction of metal ions and cationic dyes.[14] Chen et al. reported a PAA/PES polymer to promote the separation efficiency of oil/water emulsion.[10] PAA hydrogels exhibit certain potential to remove contaminants from wastewater.[15-18] However, most PAA hydrogels are prepared via polymerization to form the three-dimensional net structure.[19-21] In these cases, most carboxyl groups of PAA are wrapped inside the hydrogels, which prevents them from interacting with pollutants and greatly reduces the mass transfer efficiency.[22-23] Moreover, most of the reported hydrogels swell with water absorption; their volume and mass will increase many times after wastewater treatment, which greatly limit their application.[24-27] Therefore, we aimed to develop a novel water-insoluble PAA adsorbent with multiple functions, excellent mass transfer efficiency, recoverability, and non-swelling characteristics.

Inspired from the structural features of dandelion, we found that the immobilization of linear PAA on water-insoluble nanoparticles (NPs), which could expose carboxyl groups to come in contact with pollutants. Additionally, this structure can also effectively avoid polymer swelling without forming a three-dimensional net structure. Silica (SiO_2) NPs are water-insoluble and have many excellent properties, including excellent swelling resistance, perfect mechanical and chemical stability, non-toxicity, and low cost. Importantly, the surface of SiO_2 NPs is filled with hydroxyl group, enabling them to be used as a support of linear PAA.[28-32] Therefore, the preparation of non-swelling polymer based on SiO_2 and PAA is feasible. We hypothesized that the non-swelling SiO_2-PAA will exhibit high efficiency in simultaneously removing emulsion, cationic dyes, and heavy metal co-contaminants. Studies about the construction of PAA-based multifunctional polymers have not yet been reported to date.

Herein, we report a non-swelling SiO_2-PAA composite through the surface modification of SiO_2 using poly(acrylic acid) (PAA) under relatively mild conditions. The remaining carboxyl groups of PAA chains in the polymer were exposed to act as the binding sites for pollutant removal. Methylene blue (MB) and Cr(III) are well-known cationic dye and heavy metal, commonly used in textile, printing, and tanneries. Moreover, co-existing of the pollutants with emulsions greatly enhance the difficulties of processing. Therefore, cetyltrimethylammonium bromide (CTAB)-stabilized emulsions, typical pollutants MB and Cr(III) were investigated as model pollutants in this study. The emulsion separation ability, adsorption isotherms, and adsorption kinetics against a single MB or Cr(III) and the removal efficiency against co-

contaminants of emulsions, cationic dyes, and heavy metal were investigated to comprehensively evaluate the performance of the prepared non-swelling SiO_2-PAA.

2. EXPERIMENTAL SECTION

2.1. Materials. SiO_2 NPs, PAA (M_W = 5000, 50.0% w/v in water), N-(3-dimethyl aminopropyl)-N-ethyl carbodiimide hydrochloride (EDC), (3-Aminopropyl)trimethoxysilane (APTMOS, 97.0%), and N-hydroxysuccinimide (NHS) were acquired from Aladdin Co., Ltd. (Shanghai, China). Toluene, MB, dodecane, CTAB, and chromium sulfate were obtained from Kelong Co., Ltd. (Chengdu, China). Analytically pure reagents were used in this study.

2.2. Synthesis of SiO_2-PAA composites. The SiO_2-PAA composite, which was proposed based on the basic principles of polymerization with similar functional groups,[33-34] was synthesized via two procedures. Firstly, the amine-functionalized particle (SiO_2-APTMOS), was obtained through the reaction between hydroxy of SiO_2 NPs and alkoxy of APTMOS. Typically, SiO_2 particles (10.0 g) were dispersed in the mixture of toluene (50 mL) and APTMOS (10 mL). After reacting at 80 °C for 12 h, the prepared amine-functionalized particles (SiO_2-APTMOS) were washed with acetone and ethanol, and further dried at 80 °C. SiO_2-PAA was fabricated by immobilizing PAA on the surface of SiO_2-APTMOS through a condensation reaction between the $-NH_2$ of SiO_2-APTMOS and -COOH of PAA under catalytic conditions of EDC/NHS. Based on the results of preliminary experiments, SiO_2-APTMOS (8.0 g) was added in deionized water (50 mL). Then, 5.0 g of PAA, 2.4 g of EDC, and 1.6 g of

NHS were suspended in the mixture, then stirred at 50 °C for 6 h. At last, the prepared SiO_2-PAA was washed with ethanol and deionized water, and dried at 50 °C.

2.3. Characterization of SiO_2-PAA. SiO_2-PAA was characterized to verify its structural feature. The morphologies were analyzed using transmission electron microscopy (TEM, Titan G2 60-300, USA). The chemical structure of samples was investigated using a Thermo Fisher Scientific Nicolet 6700 FTIR spectrometer with wavenumber range of 400–4000 cm^{-1}. Composition measurement and phase analysis were performed by a PANalytical X-ray diffraction (XRD) detector with Cu $K\alpha_1$ radiation, the data were collected from 10° to 80° with 0.02626° 2θ step size and 30 ms/step counting time. The Brunauer–Emmett–Teller (BET) equation was employed to evaluate the surface area. To evaluate the organic loading in SiO_2-PAA, thermogravimetric analysis (TGA) was carried out in aPerkinElmer TGA8000 analyzer under nitrogen atmosphere with 10 °C/min heating rate from 30 °C to 800 °C. A Brookhaven NanoBrook Omni analyzer was employed to measure the zeta potentials and the droplet size distribution.

Swelling capacity is a key parameter to evaluate the practical performance of polymer adsorbents. Strong swelling capacity is disadvantageous to the practical application of polymer adsorbents. To determine the swelling degree, 1.000 g of dry SiO_2-PAA was dispersed in distilled water (100 mL) for 48 h. Then, SiO_2-PAA was weighed after removing the excess water from their surface with filter paper. The swelling ratio R was calculated using Eq. (1):

$$\text{The swelling ratio (R)} = \frac{w_2 - w_1}{w_2} \times 100\% \qquad (1)$$

where R is the percentage water absorption of SiO_2-PAA and w_1 and w_2 represent the weights of SiO_2-PAA in the dry and swollen states, respectively.

2.4. Emulsion separation performance. The surfactant-stabilized emulsion was prepared prior to separation performance tests. In brief, 10 mL of dodecane was dropped into 990 mL of deionized water containing 1.0 g of CTAB under 1000 rpm stirring. The resultant mixture was further stirred at 3000 rpm for 30 min.

The emulsion separation performance was determined as follows: SiO_2-PAA (20.0 mg) was added into emulsion (50 mL), and the mixture was shaken in a thermostatic shaker at 25 °C for 30 min. Then, a filtration procedure was performed with filter paper. The droplet size distribution, Tyndall phenomenon, and total organic carbon (TOC) before and after separation were analyzed.

2.5. Adsorption properties against MB and Cr(III). To make clear the adsorption properties of SiO_2-PAA, MB and Cr(III) were studied as the model pollutants. Adsorption experiments were carried out by mixing 10.0 mg of adsorbents with 50 mL of MB or Cr(III) solutions. The influence of pH on removal efficiencies were studied in pH range of 2.0–9.0 for MB solutions with initial concentration 10 mg/L and pH range of 2.5–5.5 for Cr(III) solutions with initial concentration 25 mg/L. The investigated pH range for Cr(III) solutions was set to avoid the hydroxide formation. Adsorption isotherm were investigated with initial concentration of MB at 10-500 mg/L and Cr(III) concentration at 5-160 mg/L. The adsorption were performed at 25 °C, 35 °C, and 45 °C within 30 min for MB and 4 h for Cr(III). Adsorption kinetic experiments were studied with MB concentrations of 10 mg/L and Cr(III) of 25 mg/L.

At designated time intervals, the adsorbents and treated water were separated using filter paper. The MB and Cr(III) concentrations in solution were analyzed by UV-vis spectroscopy at λ_{max} = 664 nm and ICP-OES.[35-36] The following Eqs. (2) and (3) were employed to calculate the removal rate (R) and adsorption capacity (Q_e, mg/g).

$$\mathrm{R} = \frac{C_0 - C_e}{C_0} \times 100\% \quad (2)$$

$$Q_e = \frac{(C_0 - C_e) \times V}{m} \quad (3)$$

where C_0 is the initial concentration of pollutants (mg/L), C_e is the residual concentration of pollutants (mg/L), m is the dose of SiO_2-PAA (g), and V represents the volume of wastewater (L).

2.6. Modeling of isotherm and kinetics for MB and Cr(III) adsorption on SiO_2-PAA. To meticulously study the adsorption process of SiO_2-PAA, the isotherms and kinetics of the adsorption process were studied. The Langmuir and Freundlich models, displayed in Eq. (4) and Eq. (5), respectively, were employed to fit with the isotherm data to comprehensively evaluate the adsorption capacity of SiO_2-PAA.[37-39] The formulas are shown as follows:

$$\text{Langmuir: } \frac{C_e}{Q_e} = \frac{1}{b \times Q_m} + \frac{C_e}{Q_m} \quad (4)$$

$$\text{Freundlich: } \log Q_e = \log k_f + \frac{1}{n} \times \log C_e \quad (5)$$

where C_e (mg/L) represents the concentration of pollutants after the adsorption equilibrium gained; Q_e (mg/g) is the adsorption count of pollutants on SiO_2-PAA at the equilibrium; b (L/mg) stands for the Langmuir constant; Q_m (mg/g) represents the maximum adsorption capacity of SiO_2-PAA; k_f and 1/n are Freundlich constants related to adsorption capacity and adsorption intensity, respectively.

The pseudo-first-order and pseudo-second-order models that shown in Eq. (6) and Eq. (7) were employed to fit with the adsorption kinetic data, and the formulas are shown as follows:[40]

$$\log\left(Q_e - Q_t\right) = \log Q_e - \frac{k_1 \times t}{2.303} \quad (6)$$

$$\frac{t}{Q_t} = \frac{1}{k_2 \times Q_e^2} + \frac{t}{Q_e} \quad (7)$$

where Q_t (mg/g) and Q_e (mg/g) represent the adsorption capacity of SiO_2-PAA against pollutants at time t and the equilibrium, respectively; k_1 (min^{-1}) and k_2 (g/mg/min) are the rate constant of pseudo-first-order and pseudo-second-order, respectively.

2.7. Desorption and reusability studies. The used SiO_2-PAA adsorbents (after adsorption of MB) were added into 10 mL of ethanol to desorb the absorbed MB. The mixture was stirred with 120 rpm at 25 °C for 10 min. SiO_2-PAA was further washed with distilled water several times for the following adsorption experiment. The removal rates of the recycled SiO_2-PAA on MB were evaluated.

The used SiO_2-PAA adsorbents (after adsorption of Cr(III)) were added into 10 mL HCl (0.05 mol/L) to remove the absorbed Cr(III). The mixture was stirred with 120 rpm at 25 °C for 1 h. Then, the distilled water was used to wash the SiO_2-PAA adsorbents several times for the following adsorption test toward Cr(III), and the removal rates were detected in all the reuse experiments.

2.8. Multicomponent removal studies of emulsion, Cr(III), and MB on SiO_2-PAA. A multicomponent solution was prepared via mixing 5 mL of dodecane, 5.0 mg of MB, 10.0 mg of Cr(III), 0.5 g of CTAB, and 495 mL of deionized water under stirring at 3000 rpm within 30 min. Then, SiO_2-PAA (20 mg) was mixed with 50 mL of multicomponent solution, and the suspension was shaken in a thermostatic shaker at 25 °C for 30 min. The mixture was further filtered with filter paper. The droplet size distribution, Tyndall phenomenon of Cr(III), and TOC before and after separation were analyzed.

3. RESULTS AND DISCUSSION

3.1. Preparation and characterization of SiO_2-PAA. The synthesis procedure of SiO_2-PAA is illustrated in Figure 1a. First, SiO_2-APTMOS was obtained via the reaction between hydroxy of SiO_2 NPs and alkoxy of APTMOS. Subsequently, SiO_2-PAA was fabricated by immobilizing PAA on the surface of SiO_2-APTMOS through a condensation reaction under catalytic conditions of EDC/NHS.

The morphologies of SiO_2 and SiO_2-PAA were analyzed using TEM. Figure 1b shows the TEM images of SiO_2, and uniform spherical particles (45 ± 3 nm) were observed. After grafting of PAA, the TEM images of the prepared SiO_2-PAA particles revealed that sufficient PAA was immobilized on the surface of SiO_2, and the diameter of spherical particles increased to 55 ± 5 nm (Figure 1c). In comparing the morphologies of SiO_2 and SiO_2-PAA, the sphere of SiO_2 remained stable during the synthesis process, which was similarly verified by the XRD patterns (Figure S1). Additionally, the specific surface area of SiO_2 decreased from 129.2 to 30.7 m^2/g after the formation of SiO_2-PAA, indicating abundant PAA was grafted on the surface of SiO_2 (Figure S2).

X-ray photoelectron spectroscopy (XPS) results were used to evaluate the chemical compositions of SiO_2 and SiO_2-PAA. In the wide scan spectra of SiO_2-PAA (Figure 2a), distinct peaks at 401.7 and 284.9 eV appeared, which corresponded to N 1s and C 1s, respectively. This finding indicated the formation of amide bond and the successful immobilization of PAA. The O 1s spectrum in SiO_2 (Figure 2b) could be curve-fitted into only one peak at approximately 532.9 eV, corresponding to the Si–O bond. By contrast, .three peaks at 531.5, 532.4, and 533.4 eV, corresponding to C=O, Si–O, and C–O, respectively,[41] were fitted in the O 1s of SiO_2-PAA (Figure 2c). The above results proved that PAA was successfully grafted on SiO_2. In addition, XPS element content analysis showed that 43.59% of C and 3.97% of N were detected in SiO_2-PAA from the surface chemical composition (Table 1), which further verified the successful preparation of SiO_2-PAA.

Figure 2d displayed the FT-IR spectra of SiO_2 and SiO_2-PAA. The bands located at 475, 798, 996 and 1103 cm^{-1} were the characteristics of bending vibration of Si–O, symmetric vibration of Si–O, bending vibration of Si–OH, and asymmetric stretching vibration of Si–O–Si, respectively. After the formation of SiO_2-APTMOS, new peak at 1515 cm^{-1} that corresponded to the N-H bending was viewed (Figure S3). In SiO_2-PAA, the peaks at approximately 2925 cm^{-1} indicated the symmetric stretching of CH_2. New band observed at 1714 cm^{-1} related to the stretching vibrations of C=O bonds in carboxyl groups, indicating the successful introduction of PAA. Additionally, absorption peaks at 1571 cm^{-1} was corresponded to the stretching vibrations of amide (CO–NH) bonds, such phenomena verified the covalent binding of PAA on the surface of SiO_2 through the formation of CO–NH between the -COOH in PAA and $-NH_2$ in

SiO_2-APTMOS. The comparation of the FT-IR results of the final product with SiO_2 and SiO_2-APTMOS further confirmed the successful introduction of PAA into the prepared SiO_2-PAA.

TG analysis was employed to evaluate the count of organic/polymer molecules grafted on SiO_2 particles (Figures 2e and 2f). In the TGA curves of the samples, the mass loss at temperatures below 150 °C were related to the evaporation of water that physically adsorbed on the particles, which were exhibited as endothermic peaks in the DTG curves. There was no other mass loss observed for SiO_2, which was revealed SiO_2 did not decompose below 800 °C, which was in according with earlier reports. TGA curves of SiO_2-PAA showed further mass loss in two steps at 150–800 °C due to the conversion of carboxyl to anhydride and polymer decomposition of PAA molecules respectively, which were shown as two endothermic peaks in their DTG curves. These results showed PAA was successfully grafted on SiO_2.

Moreover, the water uptake ratios of SiO_2-PAA were tested. The mass of SiO_2-PAA before and after soaking in deionized water were 1.000 g and 1.085 g, respectively (Figure S4). Little of water was absorbed, and the water uptake ratio was 8.5%, indicating that SiO_2-PAA had high practical application potential.

3.2. Emulsion separation. The treatment of emulsion wastewater is an intractable problem that needs to be solved immediately. Several methods and materials have been developed for emulsion separation.[42-45] The as-prepared SiO_2-PAA possesses the attractive property to separate cationic surfactant-stabilized emulsions. To study the separation property of emulsions, 20.0 mg of SiO_2-PAA was added into 50 mL of

CTBA-stabilized dodecane-in-water emulsion at 25 °C. As displayed in Figure 3a, the positively charged emulsion was cloudy and milky, whereas the filtrate was clear and transparent. No Tyndall effect was viewed in filtrate. The TOC decreased from 8300.0 mg/L to 1.3 mg/L after separation (Figure 3b). The particle size distribution of the emulsion was in the range of 200–900 nm (Figure 3c), whereas no particle was detected in the filtrate (Figure 3d), demonstrating nearly all the emulsions or surfactants were removed. The adsorption ability of SiO_2-PAA to CTAB was so strong that can make the emulsion droplets unsteady, resulting in demulsification and oil coalescence. Moreover, the coalesced oil could easily be blocked by the filter paper, which led to a high separation efficiency.

3.3. Adsorption properties of MB and Cr(III) by SiO_2-PAA

3.3.1. Effect of pH. The abundant carboxyl groups in SiO_2-PAA should contribute to the removal of pollutants. To verify the adsorption properties of SiO_2-PAA, MB and Cr(III) were chosen as pollutants. The solution pH remarkably influenced the surface charge of SiO_2-PAA, degree of ionization, and structure of pollutants is a significant factor .[46-47] Therefore, the adsorption behaviors of SiO_2-PAA to MB and Cr(III) at different pH were investigated (Figures 4a and 4b). The removal rates of SiO_2-PAA to MB and Cr(III) increased as the pH increased, and nearly unchanged at pH >4.0. This finding indicated the removal of MB and Cr(III) by SiO_2-PAA is fully dependent on the pH. As a control, the pure SiO_2 had much lower removal rates of MB and Cr(III) (less than 60.0% and 10.0%, respectively) than SiO_2-PAA. The pH of zero-point charge of SiO_2-PAA was approximately 3.4 (Figure 4c). For MB, SiO_2-PAA was protonated when pH was lower than 3.4, and the superabundant H^+ ions of SiO_2-PAA competed with MB molecules to decrease the removal rate. By contrast, SiO_2-PAA was deprotonated at higher pH values, and the electrostatic attraction between SiO_2-PAA and MB molecules led to a higher removal efficiency. For Cr(III), thermodynamic analysis indicated Cr(III) mainly exists as $CrSO_4^+$ and $CrOH^{2+}$ in the pH range of 2.5–5.5 (Figure S5). The high Cr(III) removal rates of SiO_2-PAA were ascribed to the strong complexation between Cr(III) and ionized carboxyl groups. However, the adsorption ability of SiO_2 to MB could be attributed to the electrostatic attraction between the negatively charged SiO_2 and positive charge of MB, and the weak complexation between SiO_2 and Cr(III) led to the removal of small amounts of Cr(III). In comparing SiO_2 and SiO_2-PAA, the exceptional adsorption behavior of SiO_2-PAA to MB and Cr(III) was mainly attributed to the immobilized PAA.

3.3.2. Adsorption isotherm of MB and Cr(III). The adsorption isotherm can be used to not only assess the adsorption capacity of adsorbents but also illustrate the distribution of pollutants between SiO_2-PAA and wastewater. Figure 5a illustrates the effects of initial MB concentrations on the adsorption capacity of SiO_2-PAA. The experimental data were applied to fit with the isotherm models for further investigation of adsorption characteristics (Figures 5b and S6). The correlation coefficient (R^2) of the Langmuir model was higher than that of the Freundlich model, showing the experimental data was in line with the Langmuir isotherm model well (Table S2). Based on the Langmuir isotherm model, the experimental maximum adsorption capacity (Q_m) of MB on SiO_2-PAA reached 758.6 mg/g at 45 °C. Figure 5c exhibits Qe increased with the initial concentrations of Cr(III) increasing, and the experimental maximum adsorption capacity was 178.6 mg/g at initial Cr(III) concentration of 160 mg/L at 45 °C. Although some reported material exhibited high adsorption capacity of MB,[48] the adsorption capacities for MB and Cr(III) of SiO_2-PAA was higher than those of other PAA adsorbents reported in literature, listed in Table 2.[49-53] Figures 5d and S7 show the matching results of experimental data with the isotherm models. The results indicated the adsorption process also better accorded with the Langmuir model (Table S3). The excellent adsorption of MB and Cr(III) possibly resulted from the abundant carboxyl groups and divergent structure of SiO_2-PAA, which can enhance the mass transfer and promote MB and Cr(III) to be adsorbed on SiO_2-PAA rapidly. The removal rates of MB and Cr(III) increased with increasing temperature, showing the removal of MB and Cr(III) by SiO_2-PAA was an endothermic reaction.

The effects of temperature on removal of MB and Cr(III) by SiO_2-PAA were studied at 298 K, 308 K, and 318 K (Text S1, Figure S8, and Table S4 in the supplementary material). The ΔG values are negative for MB and Cr(III) removal, demonstrating the removal of MB and Cr(III)are spontaneous processes. The positive ΔH values indicate the adsorption are possibly endothermic process, and the adsorption can be improved by increasing the temperature. The positive ΔS values indicate the disorder on the SiO_2-PAA/wastewater interface are enhanced during the adsorption process.

3.3.3. Adsorption kinetics of MB and Cr(III). The adsorption kinetics were studied to understand the adsorption ability of SiO_2-PAA to MB and Cr(III). The effect of reaction time on the adsorption capacity of SiO_2-PAA of MB was illustrated in Figure

6a. More than 80.0% of MB was removed within 0.5 min, then 99.9% of MB were removed at 30 min and the adsorption equilibrium was achieved. The inserted picture showed MB solution was colorless after adsorption (see inset of Figure 6a), showing nearly all MB were removed by SiO_2-PAA. Pseudo-first-order and pseudo-second-order models were employed to study the adsorption kinetics of MB removal by SiO_2-PAA (Figures S9 and 6b), and the kinetic parameters were calculated and listed in Table S5. The high R^2 of 0.9998 indicated that the experimental data accorded with the pseudo-second-order kinetic model.

Figure 6c depicts the effect of adsorption time on the removal rate of pollutants by SiO_2-PAA at Cr(III) concentration of 25 mg/L. The Cr(III) removal rate gradually increased with increasing reaction time. Then, the adsorption equilibrium was achieved at 6 h. Pseudo-first-order and pseudo-second-order kinetic models were used to study the adsorption kinetics of Cr(III) (Figures S10 and 6d). The experimental data matched well with the pseudo-second-order kinetic model (Table S6).

3.3.4. Desorption and regeneration. Reusability is a vital prerequisite for practical use of adsorbents.[33,54] At the end of adsorption experiments, MB-loaded SiO_2-PAA were soaked into ethanol (10 mL) due to the better solubility of MB in ethanol. After rinsing with deionized water and drying, the regenerated SiO_2-PAA was employed to perform another adsorption of pollutants, and the recycling results are displayed in Figure 7. The adsorption capacity still remained 91.5% after five cycles of regeneration, indicating the exceptional reusability of SiO_2-PAA.

Approximately 0.05 mol/L of HCl was exploited to regenerate Cr(III)-saturated

SiO_2-PAA. After accomplishing the regeneration, SiO_2-PAA was further used for another adsorption experiment. Figure 7 shows the adsorption rates for five cycles of adsorption process, and the results demonstrated that SiO_2-PAA had outstanding reusability. After the five cycle, the adsorption capacity of SiO_2-PAA for Cr(III) still remained 90.2% of the first cycle.

3.3.5. Adsorption mechanism. SiO_2-PAA contains abundant carboxyl groups that can bind with MB and Cr(III). Thus, to assess the adsorption performance of SiO_2-PAA on MB and Cr(III) removal, XPS characterization was performed on SiO_2-PAA before and after adsorption. In the wide scan spectra of SiO_2-PAA-Cr(III) (Figure 8a), an obvious peak appeared at 577.4 eV, which corresponded to Cr 2p after adsorption, demonstrating that Cr(III) was resoundingly adsorbed. The O1s spectra of free SiO_2-PAA clearly indicated that three parts were ascribed to C=O at 531.5 eV, Si–O at 532.4 eV, and C–O at 533.4 eV, respectively (Figure 8b). After adsorption of MB, the C–O peak shifted from 533.4 eV to 533.1 eV, and the peak intensity slightly increased (Figure 8c). While, after adsorption of Cr(III), the C–O peak shifted from 533.4 eV to 534.1 eV with peak intensity markedly decreased (Figure 8d). These phenomena indicated that carboxyl groups in SiO_2-PAA played a vital role in MB and Cr(III) adsorption. The different variation tendency of C–O peak after adsorption of MB and Cr(III) possibly result from their different binding interactions with carboxyl groups.

Several studies show that the mass loss at 250 °C in the TGA and DTG curves of PAA corresponded to the conversion of free carboxyl to anhydride during heating.[55] Therefore, the TGA and DTG curves of SiO_2-PAA, SiO_2-PAA-MB, and SiO_2-PAA-

Cr(III) were employed to study the removal of MB and Cr(III) on SiO_2-PAA (Figures 8e and 8f). The endothermic peak of SiO_2-PAA at approximately 250 °C changed considerably after adsorbing MB and Cr(III), indicating the bonding forms of carboxyl groups with MB or Cr(III) were different. The weight loss of SiO_2-PAA associated with carboxyl conversion was 10.5 wt.%. For SiO_2-PAA-MB, the weight loss at approximately 250 °C decreased to 7.7 wt.%. This finding was because the removal of MB mainly depended on the electrostatic attraction between the carboxyl groups of SiO_2-PAA and the quaternary ammonium groups of MB; however, this chemical bond broke during heating. For SiO_2-PAA-Cr(III), the decomposition peak around 250 °C in the DTG curve almost disappeared (4.1 wt.%, Figure 8f), indicating that few free carboxyl groups were present in SiO_2-PAA-Cr(III). This finding should be attributed to the formation of the coordinate bond between free carboxyl and Cr(III).

3.4. Multicomponent removal studies of emulsion, Cr(III), and MB by SiO_2-PAA. To verify the multifunctional nature of SiO_2-PAA, 20.0 mg of SiO_2-PAA was added into 50 mL of the mixed solution containing CTAB-stabilized emulsion, MB, and Cr(III) at 25 °C for 30 min. As displayed in Figure 9a, the mixed solution transformed from galactoid and blue to clear and colorless, and no Tyndall effect was observed, implying that the emulsion was fully separated and that MB was completely adsorbed. To confirm this finding, the DLS curves of the mixed solution and the filtrate were measured (Figure 9b). No particle was detected in the filtrate (Figure 9c). Furthermore, the TOC concentration of the filtrate decreased to 3.4 mg/L (Figure 9d). Cr(III) and MB were also not detected in the filtrate (Figures 9e and 9f). These results demonstrate that the separation rate for emulsion was relatively high, and MB and Cr(III) had been completely adsorbed by SiO_2-PAA. SiO_2-PAA proved to be a potential multifunctional material for wastewater treatment.

4. CONCLUSIONS

In this work, a novel multifunctional and excellent SiO_2-PAA with non-swelling property was fabricated by grafting the linear PAA onto the surface of SiO_2. The as-prepared SiO_2-PAA could realize excellent surfactant-stabilized emulsion separation and exceptional adsorption behavior of cationic dye MB and heavy metal ion Cr(III). This phenomenon was mainly ascribed to the fact that SiO_2-PAA increased the mass transfer efficiency without forming a three-dimensional network structure, and almost all carboxyl groups were exposed to pollutants. Moreover, the mechanism of MB removal could be attributed to electrostatic and hydrogen bonding interactions between MB and SiO_2-PAA. The removal of Cr(III) on SiO_2-PAA was mainly ascribed to the formation of complex by carboxyl of PAA and Cr(III). Given these findings, the designed SiO_2-PAA is a potential e material for wastewater treatment. The results of this study will provide new references for functional integration in environmentally friendly multifunctional materials.

FIGURES

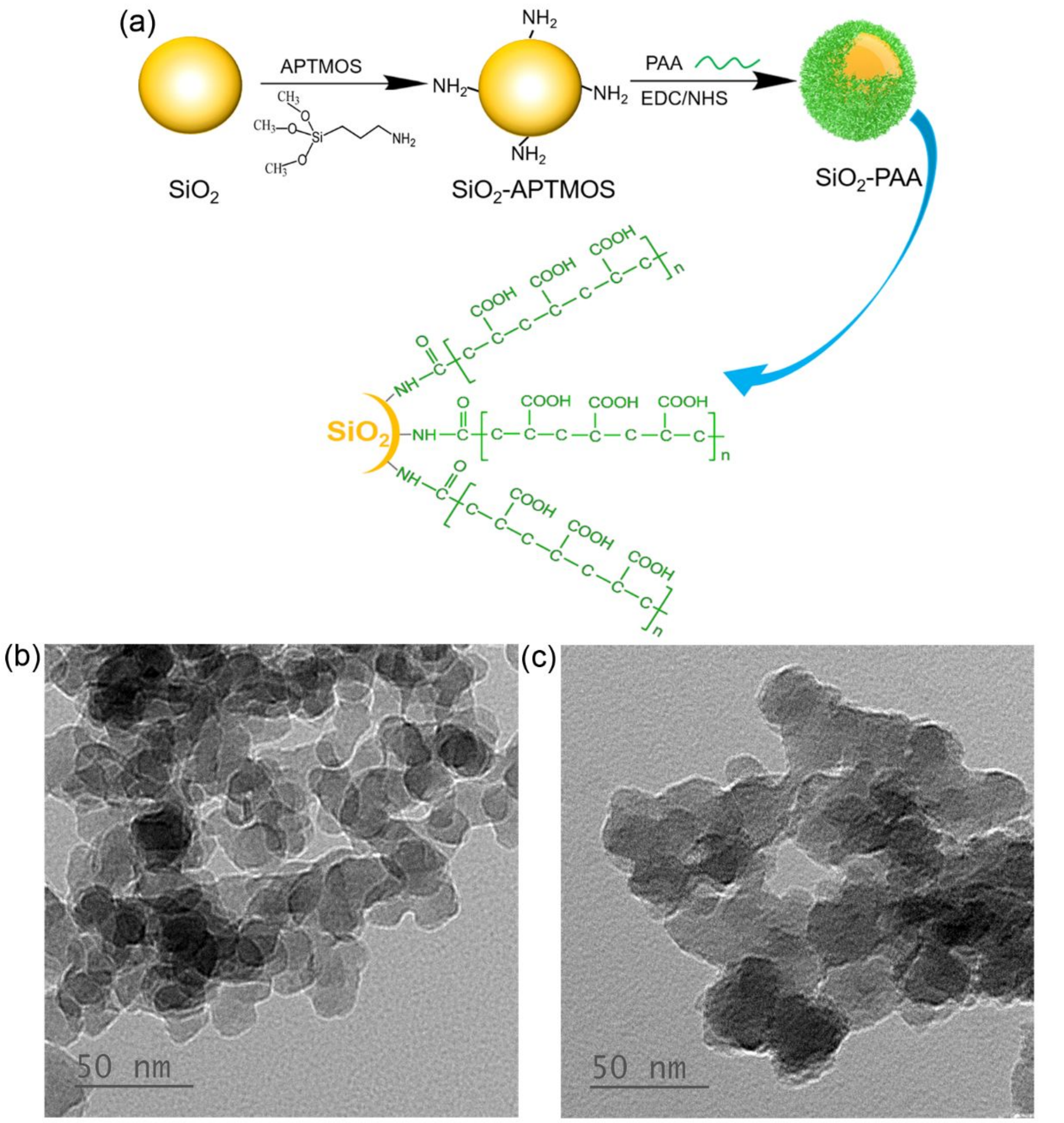

Figure 1 (a) Synthesis of the SiO_2-PAA via the surface modification of SiO_2 with sufficient carboxyl groups of polyacrylic acid (PAA); TEM images of (b) SiO_2 and (c) SiO_2-PAA.

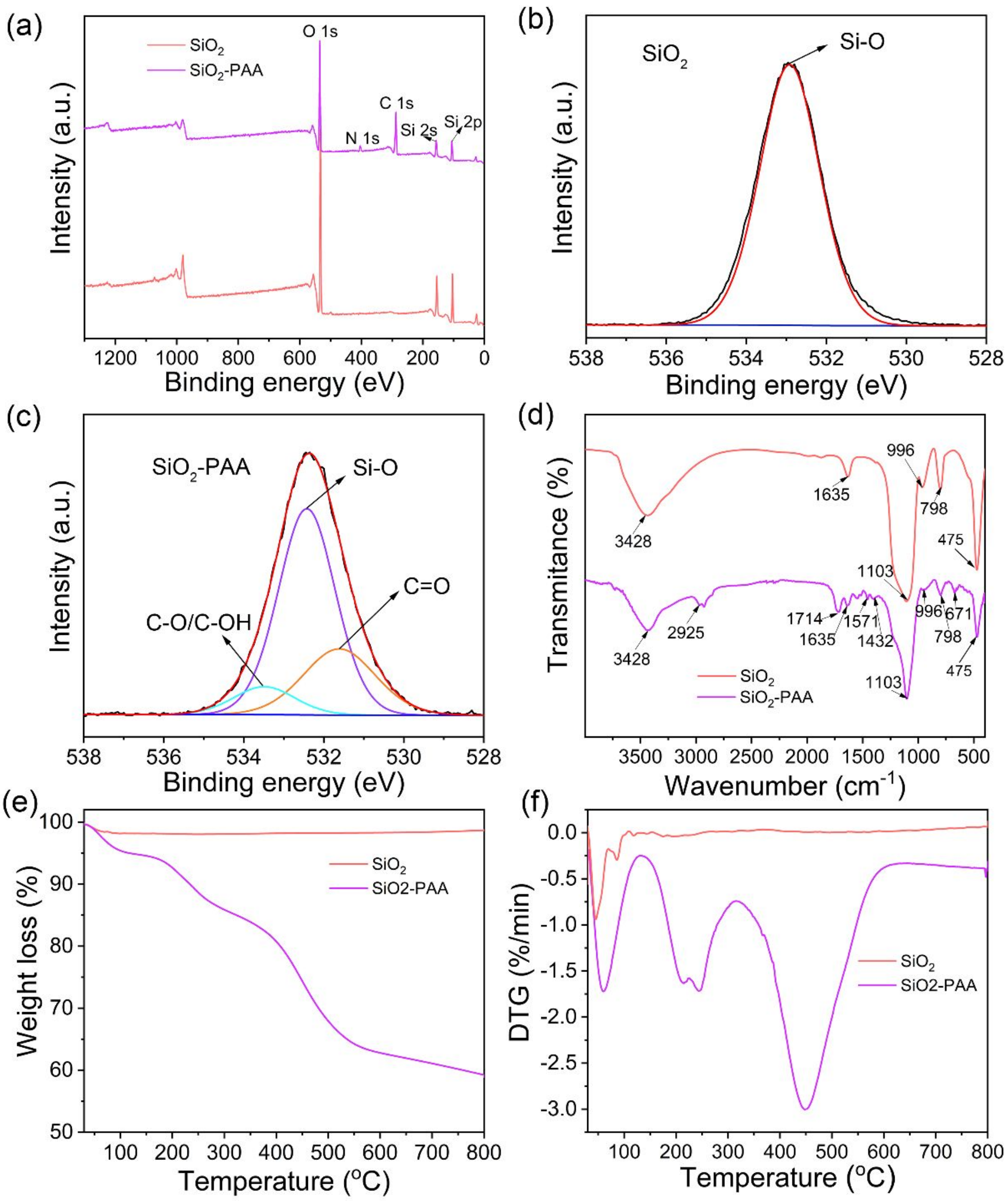

Figure 2 (a) XPS wide spectra of SiO_2 and SiO_2-PAA; O 1s high-resolution spectra of (b) SiO_2 and (c) SiO_2-PAA; (d) FTIR spectra, (e) TGA, and (f) DTG curves of SiO_2 and SiO_2-PAA.

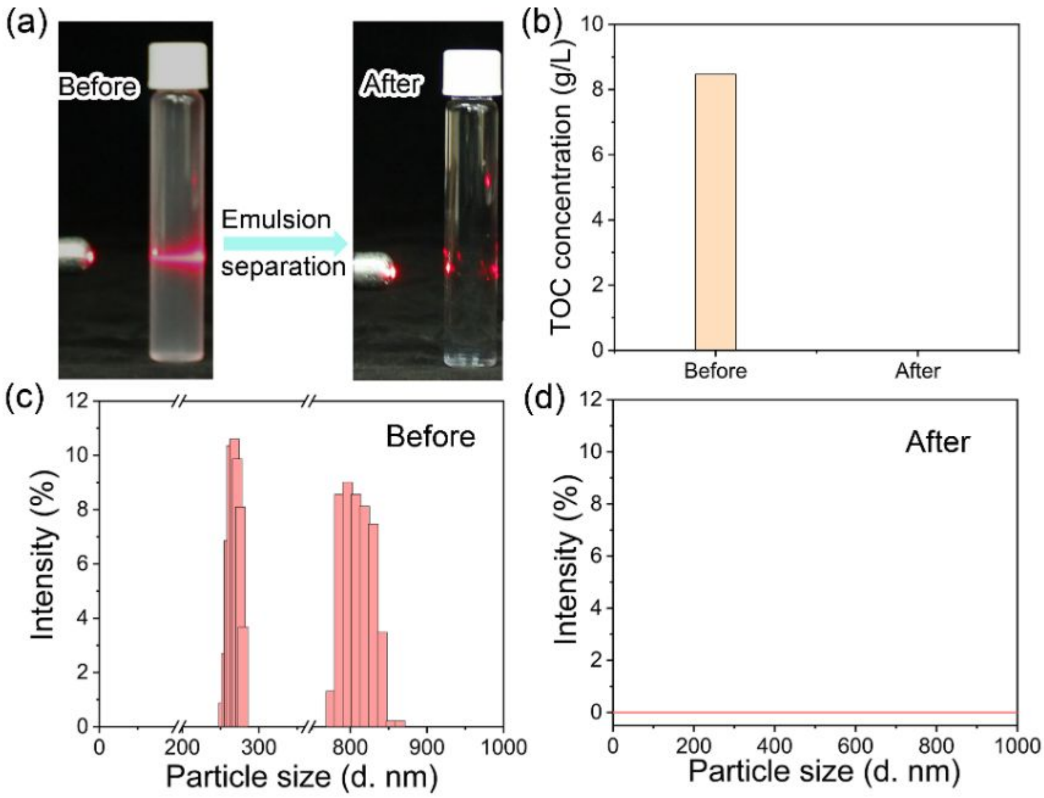

Figure 3 (a) Digital pictures of the emulsion before and after separation; (b) TOC concentration of the emulsion before and after separation; Particle sizes of the emulsion (c) before and (d) after separation.

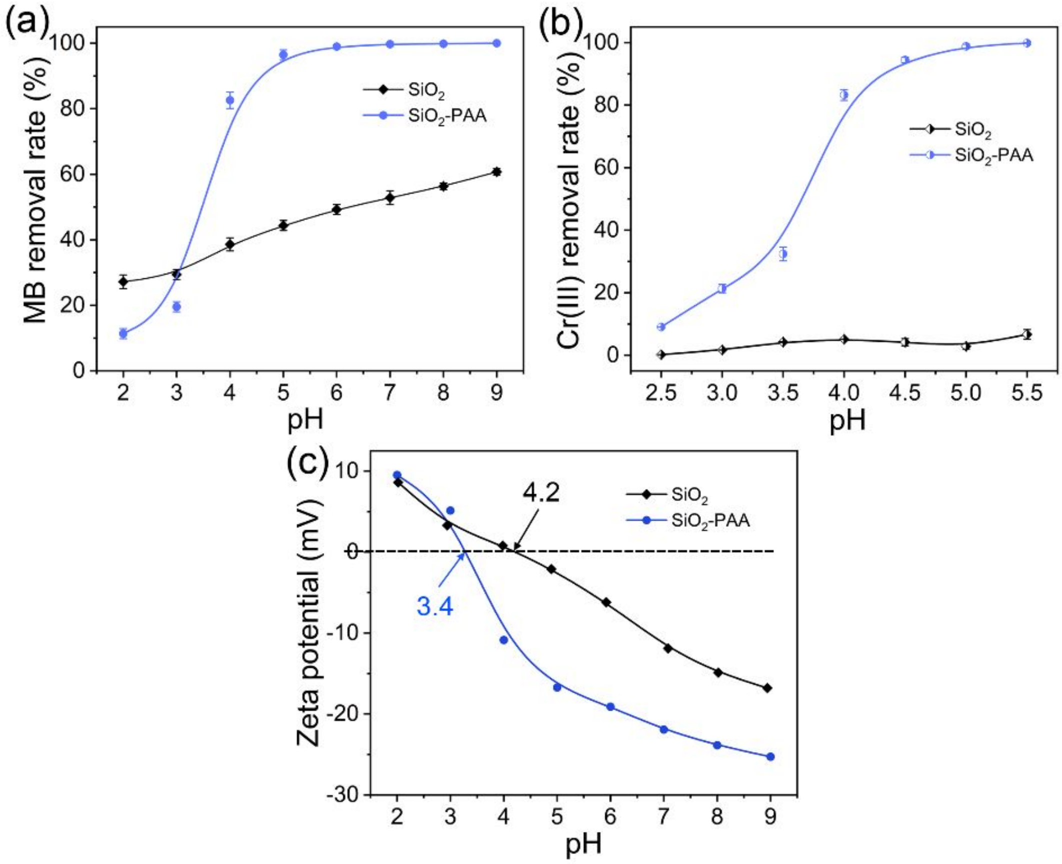

Figure 4 Effect of pH values on the removal efficiency of (a) MB and (b) Cr(III)(For MB: 10 mg/L MB and 0.2 g/L adsorbent were stirred at 25 °C for 30 min; For Cr(III): 25 mg/L Cr(III) and 0.2 g/L adsorbent were stirred at 25 °C for 4 h.); (c) Zeta potential of SiO_2 and SiO_2-PAA.

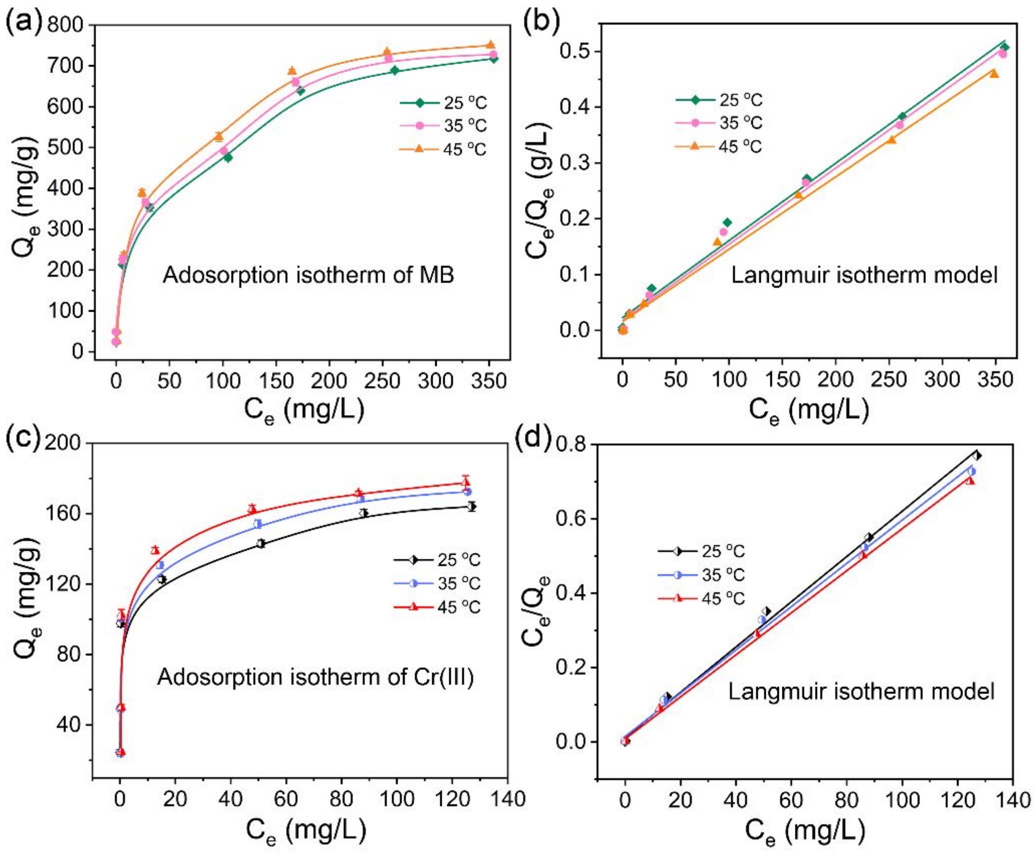

Figure 5 (a) Adsorption isotherm of MB on SiO_2-PAA; (b) Langmuir model fitted adsorption data of MB; (c) Adsorption isotherm of Cr(III) on SiO_2-PAA; (d) Langmuir model fitted adsorption data of Cr(III). (For MB: pH = 5.0, SiO_2-PAA dose was 0.2 g/L, t = 30 min; For Cr(III): pH = 5.0, SiO_2-PAA dose was 0.2 g/L, t = 4 h.)

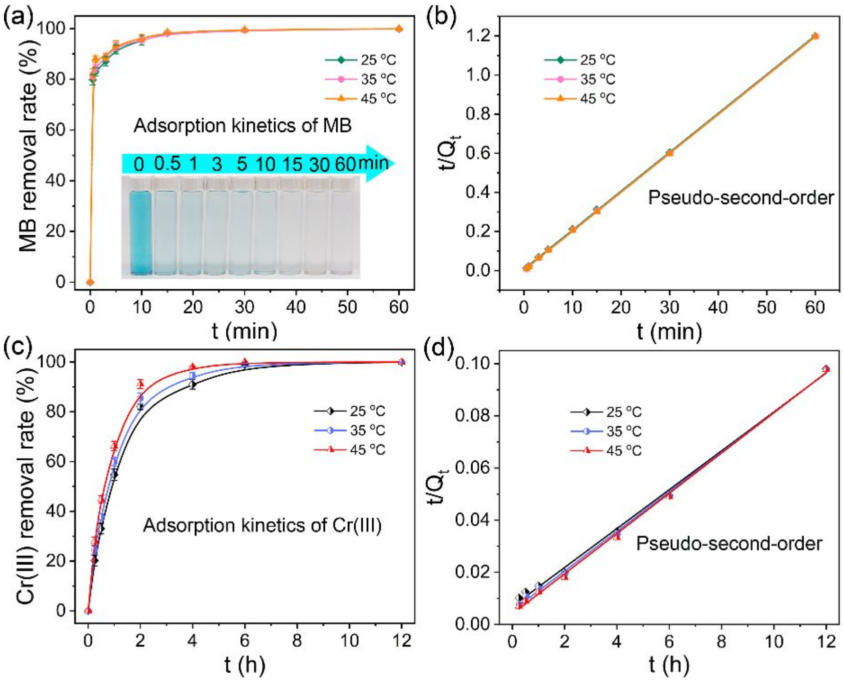

Figure 6 (a) Kinetics datas of MB on SiO_2-PAA. Inserting photo shows the color changes of MB solution by SiO_2-PAA adsorption with the changes of adsorption time; (b) Pseudo-second order model fitted kinetics datas of MB; (c) Kinetics data of Cr(III) on SiO_2-PAA; (d) Pseudo-second order model fitted kinetics datas of Cr(III). (For MB: pH = 5.0, 0.2 g/L adsorbent dose, 10 mg/L MB; For Cr(III): pH = 5.0, 0.2 g/L adsorbent dose, 25 mg/L Cr(III).)

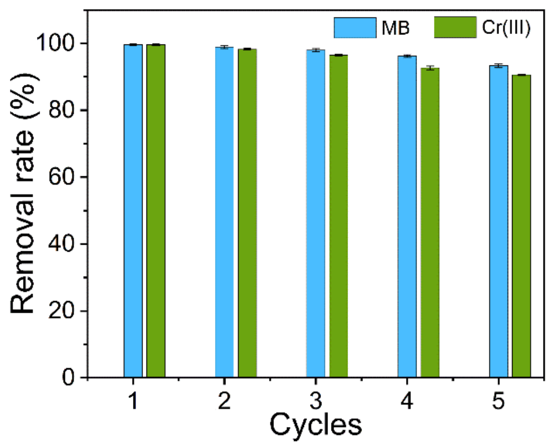

Figure 7 Reusability of SiO_2-PAA for MB and Cr(III) adsorption.

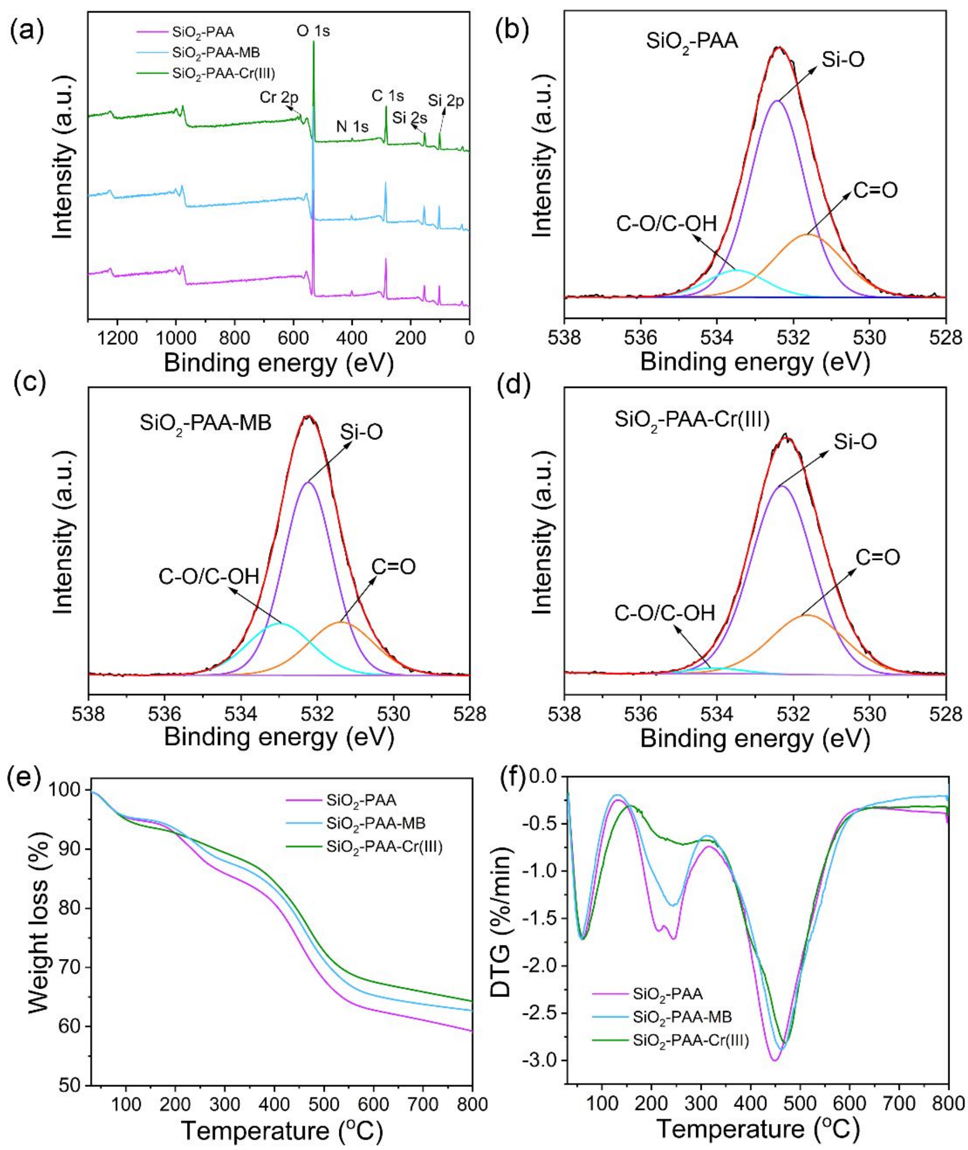

Figure 8 (a) XPS wide spectra of SiO_2-PAA, SiO_2-PAA-MB, and SiO_2-PAA-Cr(III); O 1s high-resolution spectra of (b) SiO_2-PAA, (c) SiO_2-PAA-MB, and (d) SiO_2-PAA-Cr(III); (e) TG and (f) DTG curves of SiO_2-PAA, SiO_2-PAA-MB andSiO_2-PAA-Cr(III).

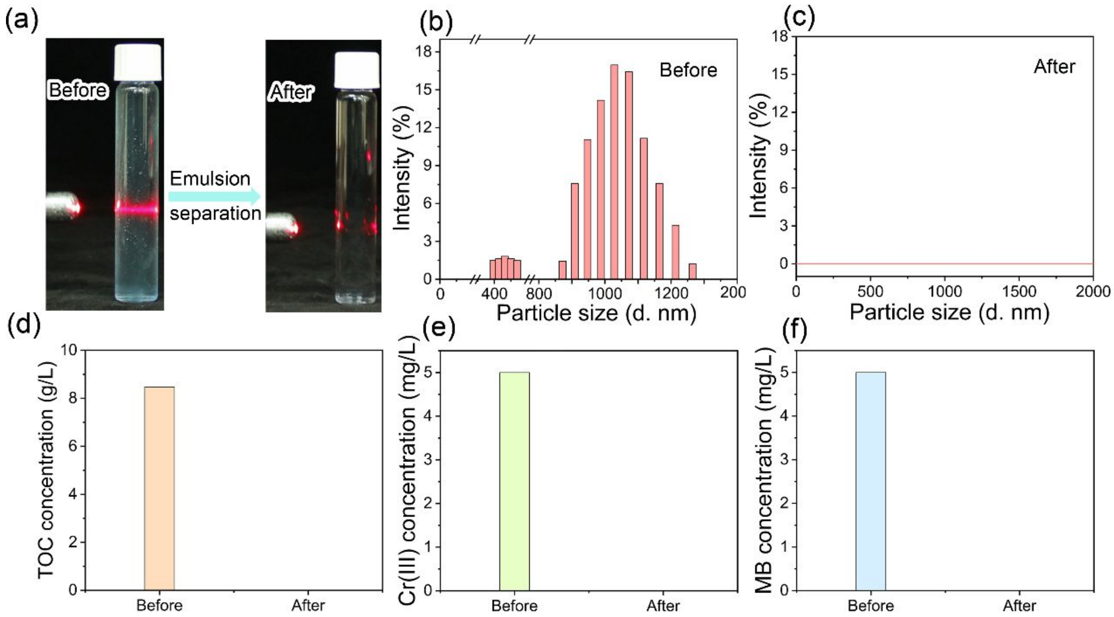

Figure 9 (a) Digital pictures of the mixed solution before and after separation; DLS data of the solution (b) before and (c) after separation; (d) TOC concentration of the mixed solution before and after separation; (e) Cr(III) and (f) MB concentrations in the mixed solution before and after separation.

TABLES

Table 1 Element content analysis of SiO_2 and SiO_2-PAA by XPS.

Sample	C-Atomic%	O-Atomic%	Si-Atomic%	N-Atomic%
SiO_2	0.00	59.82	40.18	0.00
SiO_2-PAA	43.59	37.28	15.16	3.97

Table 2 Maximum adsorption capacities for adsorption MB or Cr(III) onto various PAA adsorbents.

Adsorbent	Adsorption capacity	Reference
Sodium alginate-crosslinked-poly(acrylic acid)/TiO_2 O/I-hydrogels	2257.3 mg/g for MB	[48]
Magnetic poly(aspartic acid)-poly(acrylic acid)hydrogel	357.1 mg/g for MB	[49]
Corn stalk fibers grafted polyacrylic acid	370.0 mg/g for MB	[50]
Xanthan gum-cl-poly acrylic acid/oxidized MWCNTs	521.0 mg/g for MB	[51]
Soybean dregs-poly(acrylic acid) hydrogel	41.7 mg/g for Cr(III)	[52]
Fe_3O_4 nanoparticle grafted with polyacrylic acid	54.1 mg/g for Cr(III)	[53]
SiO_2-PAA	758.6 mg/g for MB	This work
SiO_2-PAA	178.6 mg/g for Cr(III)	This work

ASSOCIATED CONTENT

Supporting Information.

Thermodynamics of Cr(III) and MB adsorption (Text S1); XRD patterns of SiO_2 (a) and SiO_2-PAA (b) (Figure S1). N_2 adsorption-desorption isotherms of (a) SiO_2 and (b) SiO_2-PAA (Figure S2). Digital pictures of SiO_2-PAA before (left) and after (right) soaking in deionized water (Figure S4). Distribution of Cr(III) species in aqueous solution at different pH (Visual MINEQL 2.40b version, NIST database, initial concentration of Cr(III) = 0.5mmol/L) (Figure S5). Adsorption data of MB fitted with the Freundlich model (Figure S6). Adsorption data of Cr(III) fitted with the Freundlich model (Figure S7). Van't Hoff linear plot of lnK vs. 1/T (Figure S8). Adsorption data of MB fitted with the pseudo-first order kinetic model (Figure S9). Adsorption data of Cr(III) fitted with the pseudo-first order kinetic model (Figure S10). Effect of pH on the removal of Cr(VI) and distribution of Cr(VI) species in aqueous solution at different pH (Visual MINEQL 2.40b version, NIST database, initial concentration of Cr(VI) = 0.5mmol/L) (Figure S11). The LC-MS results of the MB polluted solution before adsorption and after adsorption (Figure S12). Effect of the mass ratio of SiO_2-APTMOS to PAA on MB removal (Table S1). Parameters for Langmuir and Freundlich isotherm models of MB (Table S2). Parameters for Langmuir and Freundlich isotherm models of Cr(III) (Table S3). Calculated thermodynamic parameters for MB and Cr(III) adsorption under different conditions on SiO_2-PAA (Table S4). Parameters of kinetic models for the adsorption of MB on SiO_2-PAA (Table S5). Parameters of kinetic models for the adsorption of Cr(III) on SiO_2-PAA (Table S6).

AUTHOR INFORMATION

Corresponding Author

* Electronic mail: zhouamao2004@126.com (J, Z).

ACKNOWLEDGMENT

This work was supported by the National Key Research and Development Program of China (2018YFC1802201), the National Natural Science Foundation of China (21476149), the Innovation Team Program of Science & Technology Department of Sichuan Province (Grant 2017TD0010) and the Key R&D Program of Zhejiang Province (2017C03055). We also appreciate Dr. Bo Gao from the Analytical & Testing Center of Sichuan University for help with LC-MS characterization.

REFERENCES

(1) Wu, Y.; Chen, L.; Long, X. W.; Zhang, X. L.; Pan, B. C.; Qian, J. S. Multi-functional magnetic water purifier for disinfection and removal of dyes and metal ions with superior reusability. *J. Hazard. Mater.* **2018,** *347,* 160-167.

(2) Jiang, J.; Zhang, Q.; Zhan, X.; Chen, F. A multifunctional gelatin-based aerogel with superior pollutants adsorption, oil/water separation and photocatalytic properties. *Chem. Eng. J.* **2019,** *358,* 1539-1551.

(3) Barylak, M.; Cendrowski, K.; Mijowska, E. Application of carbonized metal-organic framework as efficient adsorbent of cationic dye. *Ind. Eng. Chem. Res.* **2018,** *57,* 4867-4879.

(4) Sun, H.; Jiang, J. H.; Xiao, Y. F.; Du, J. Z. Efficient removal of polycyclic aromatic hydrocarbons, dyes, and heavy metal ions by a homopolymer vesicle. *Acs Appl. Mater. Interfaces* **2018,** *10,* 713-722.

(5) Soyekwo, F.; Liu, C.; Zhao, L.; Wen, H.; Huang, W.; Cai, C.; Kanagaraj, P.; Hu, Y. Nanofiltration membranes with metal cation-immobilized aminophosphonate

networks for efficient heavy Mmetal ion removal and organic dye degradation. *Acs Appl. Mater. Interfaces* **2019,** *11,* 30317-30331.

(6) Li, J.; Li, X. D.; Hayat, T.; Alsaedi, A.; Chen, C. L. Screening of zirconium-based metal-organic frameworks for efficient simultaneous removal of antimonite (Sb(III)) and antimonate (Sb(V)) from aqueous solution. *Acs Sustain. Chem. Eng.* **2017,** *5,* 11496-11503.

(7) Huang, L. J.; Cai, J. Y.; He, M.; Chen, B. B.; Hu, B. Room-temperature synthesis of magnetic metal-organic frameworks composites in water for efficient removal of methylene blue and As(V). *Ind. Eng. Chem. Res.* **2018,** *57,* 6201-6209.

(8) Amano, Y.; Nakagawa, Y.; Ohta, S.; Ito, T. Ion-responsive fluorescence resonance energy transfer between grafted polyacrylic acid arms of star block copolymers. *Polymer* **2018,** *137,* 169-172.

(9) Qi, Y.; Chenying, L.; Henghui, H.; Hualin, C.; Bailing, L. Waterborne carboxyl-terminated hyperbranched oligomer polyester ligand: aynthesis, characterization and chelation with chromium(III). *J. Mol. Struct.* **2017,** *1143,* 371-377.

(10) Chen, S. Q.; Lv, C. Y.; Hao, K.; Jin, L. Q.; Xie, Y.; Zhao, W. F.; Sun, S. D.; Zhang, X.; Zhao, C. S. Multifunctional negatively-charged poly (ether sulfone) nanofibrous membrane for water remediation. *J. Colloid Interface Sci.* **2019,** *538,* 648-659.

(11) Mathew, M. L.; Gopalakrishnan, A.; Aravindakumar, C. T.; Aravind, U. K. Low - cost multilayered green fiber for the treatment of textile industry waste water. *J. Hazard. Mater.* **2019,** *365,* 297-305.

(12) Li, T.; Zhang, W. M.; Zhai, S.; Gao, G. D.; Ding, J.; Zhang, W. B.; Liu, Y.; Zhao, X.; Pan, B. C.; Lv, L. Efficient removal of nickel(II) from high salinity wastewater by a novel PAA/ZIF-8/PVDF hybrid ultrafiltration membrane. *Water Res.* **2018,** *143,* 87-98.

(13) Su, S. Z.; Chen, R. R.; Liu, Q.; Liu, J. Y.; Zhang, H. S.; Li, R. M.; Zhang, M. L.; Liu, P. L.; Wang, J. High efficiency extraction of U(VI) from seawater by incorporation of polyethyleneimine, polyacrylic acid hydrogel and Luffa cylindrical

fibers. *Chem. Eng. J.* **2018,** *345,* 526-535.

(14) Huang, X. L.; Zhou, D. X.; Wang, Y. L.; He, C.; Zhao, W. F.; Sun, S. D.; Zhao, C. S. A green approach towards functional hydrogel particles from synthetic polymers via spherical capsule mini-reactors. *Chem. Eng. J.* **2019,** *359,* 1360-1371.

(15) Hu, X. S.; Liang, R.; Sun, G. X. Super-adsorbent hydrogel for removal of methylene blue dye from aqueous solution. *J. Mater. Chem. A* **2018,** *6,* 17612-17624.

(16) Ding, J. Z.; Li, Q.; Xu, X.; Zhang, X. J.; Su, Y.; Yue, Q. Y.; Gao, B. Y. A wheat straw cellulose-based hydrogel for Cu(II) removal and preparation copper nanocomposite for reductive degradation of chloramphenicol. *Carbohyd. Poly.* **2018,** *190,* 12-22.

(17) Zhou, G. Y.; Luo, J. M.; Liu, C. B.; Chu, L.; Crittenden, J. Efficient heavy metal removal from industrial melting effluent using fixed-bed process based on porous hydrogel adsorbents. *Water Res.* **2018,** *131,* 246-254.

(18) Wang, X. H.; Wang, Y. Y.; Hou, H. Q.; Wang, J. J.; Hao, C. Ultrasonic method to synthesize glucan-g-poly(acrylic acid)/sodium lignosulfonate hydrogels and studies of their adsorption of Cu^{2+} from aqueous solution. *Acs Sustain. Chem. Eng.* **2017,** *5,* 6438-6446.

(19) Han, Q. Q.; Chen, L.; Li, W. X.; Zhou, Z. Y.; Fang, Z.; Xu, Z. W.; Qian, X. M. Self-assembled three-dimensional double network graphene oxide/polyacrylic acid hybrid aerogel for removal of Cu^{2+} from aqueous solution. *Environ. Sci. Pollut. Res.* **2018,** *25,* 34438-34447.

(20) Jiang, L. P.; Liu, P. Novel magnetic fly ash/poly(acrylic acid) composite microgel for selective adsorption of Pb(II) ion: synthesis and evaluation. *Ind. Eng. Chem. Res.* **2014,** *53,* 2924-2931.

(21) Wang, M. X.; Chen, Y. M.; Gao, Y.; Hu, C.; Hu, J.; Tan, L.; Yang, Z. M. Rapid self-recoverable hydrogels with high toughness and excellent conductivity. *Acs Appl. Mater. Interfaces* **2018,** *10,* 26610-26617.

(22) Paulino, A. T.; Belfiore, L. A.; Kubota, L. T.; Muniz, E. C.; Almeida, V. C.; Tambourgi, E. B. Effect of magnetite on the adsorption behavior of Pb(II), Cd(II), and

Cu(II) in chitosan-based hydrogels. *Desalination* **2011,** *275,* 187-196.

(23) Liu, C.; Zhang, Y.; Huang, J. L. Well-defined star polymers with mixed-arms by sequential polymerization of atom transfer radical polymerization and reverse addition-fragmentation chain transfer on a hyperbranched polyglycerol core. *Macromolecules* **2008,** *41,* 325-331.

(24) Wang, M.; Li, X.; Zhang, T. H.; Deng, L.; Li, P. Y.; Wang, X. F.; Hsiao, B. S. Eco-friendly poly(acrylic acid)-sodium alginate nanofibrous hydrogel: A multifunctional platform for superior removal of Cu(II) and sustainable catalytic applications. *Colloid. Surface. A* **2018,** *558,* 228-241.

(25) Jana, S.; Ray, J.; Jana, D.; Mondal, B.; Bhanja, S. K.; Tripathy, T. Removal of vanadium (IV) from water solution by sulfated Katira gum-cl-poly (acrylic acid) hydrogel. *Colloid. Surface. A* **2019,** *566,* 70-83.

(26) Meng, Q.; Peng, B.; Shen, C. Synthesis of F127/PAA hydrogels for removal of heavy metal ions from organic wastewater. *Colloid. Surf. B-Biointerfaces* **2018,** *167,* 176-182.

(27) Chitpong, N.; Husson, S. M. Polyacid functionalized cellulose nanofiber membranes for removal of heavy metals from impaired waters. *J. Membr. Sci.* **2017,** *523,* 418-429.

(28) Prete, M. C.; Tarley, C. R. T. Bisphenol A adsorption in aqueous medium by investigating organic and inorganic components of hybrid polymer (polyvinylpyridine/SiO_2/APTMS). *Chem. Eng. J.* **2019,** *367,* 102-114.

(29) Karami, S.; Zeynizadeh, B. Reduction of 4-nitrophenol by a disused adsorbent: EDA-functionalized magnetic cellulose nanocomposite after the removal of Cu^{2+}. *Carbohyd. Poly.* **2019,** *211,* 298-307.

(30) Zheng, H.; Zhou, L. M.; Liu, Z. R.; Le, Z. G.; Ouyang, J. B.; Huang, G. L.; Shehzad, H. Functionalization of mesoporous Fe_3O_4@SiO_2 nanospheres for highly efficient U(VI) adsorption. *Microporous Mesoporous Mat.* **2019,** *279,* 316-322.

(31) Ding, S. Y.; Zhang, L. L.; Li, Y.; Hou, L. A. Fabrication of a novel polyvinylidene fluoride membrane via binding SiO_2 nanoparticles and a copper

ferrocyanide layer onto a membrane surface for selective removal of cesium. *J. Hazard. Mater.* **2019,** *368,* 292-299.

(32) Han, B. W.; Cai, W. Q.; Yang, Z. C. Easily regenerative carbon/boehmite composites with enhanced cyclic adsorption performance toward methylene blue in batch and continuous aqueous systems. *Ind. Eng. Chem. Res.* **2019,** *58,* 6635-6643.

(33) Tang, Y.; Li, M.; Mu, C.; Zhou, J.; Shi, B. Ultrafast and efficient removal of anionic dyes from wastewater by polyethyleneimine-modified silica nanoparticles. *Chemosphere* **2019,** *229,* 570-579.

(34) Luckanagul, J. A.; Pitakchatwong, C.; Ratnatilaka Na Bhuket, P.; Muangnoi, C.; Rojsitthisak, P.; Chirachanchai, S.; Wang, Q.; Rojsitthisak, P. Chitosan-based polymer hybrids for thermo-responsive nanogel delivery of curcumin. *Carbohydr Polym* **2018,** *181,* 1119-1127.

(35) Li, J. Q.; Zheng, L.; Li, L. P.; Xian, Y. Z.; Jin, L. T. Fabrication of TiO_2/Ti electrode by laser-assisted anodic oxidation and its application on photoelectrocatalytic degradation of methylene blue. *J. Hazard. Mater.* **2007,** *139,* 72-78.

(36) Baldermann, A.; Landler, A.; Mittermayr, F.; Letofsky-Papst, I.; Steindl, F.; Galan, I.; Dietzel, M. Removal of heavy metals (Co, Cr, and Zn) during calcium-aluminium-silicate-hydrate and trioctahedral smectite formation. *J. Mater. Sci.* **2019,** *54,* 9331-9351.

(37) Perumal, S.; Atchudan, R.; Yoon, D. H.; Joo, J.; Cheong, I. W. Spherical chitosan/gelatin hydrogel particles for removal of multiple heavy metal ions from wastewater. *Ind. Eng. Chem. Res.* **2019,** *58,* 9900-9907.

(38) Chaudhary, M.; Rawat, S.; Jain, N.; Bhatnagar, A.; Maiti, A. Chitosan-Fe-Al-Mn metal oxyhydroxides composite as highly efficient fluoride scavenger for aqueous medium. *Carbohyd. Poly.* **2019,** *216,* 140-148.

(39) Jiang, Y.; Liu, C.; Huang, A. EDTA-functionalized covalent organic framework for the removal of heavy-metal ions. *Acs Appl. Mater. Interfaces* **2019,** *11,* 32186-32191.

(40) Huang, D.; Xu, B. L.; Wu, J. Z.; Brookes, P. C.; Xu, J. M. Adsorption and

desorption of phenanthrene by magnetic graphene nanomaterials from water: roles of pH, heavy metal ions and natural organic matter. *Chem. Eng. J.* **2019,** *368,* 390-399.

(41) Ma, J.; Ma, Y.; Yu, F.; Dai, X. H. Rotating magnetic field-assisted adsorption mechanism of pollutants on mechanically strong sodium alginate/graphene/L-cysteine beads in batch and fixed-bed column systems. *Environ. Sci. Technol.* **2018,** *52,* 13925-13934.

(42) Barrejon, M.; Syrgiannis, Z.; Burian, M.; Bosi, S.; Montini, T.; Fornasiero, P.; Amenitsch, H.; Prato, M. Cross-linked carbon nanotube adsorbents for water treatment: tuning the sorption capacity through chemical functionalization. *Acs Appl. Mater. Interfaces* **2019,** *11,* 12920-12930.

(43) Hong, X.; Huang, X. J.; Gao, Q. L.; Wu, H. M.; Guo, Y. Z.; Huang, F.; Fang, F.; Huang, H. T.; Chen, D. J. Microstructure-performance relationships of hollow-fiber membranes with highly efficient separation of oil-in-water emulsions. *J. Appl. Polym. Sci.* **2019,** *136,* 47615.

(44) Tan, L. L.; Han, N.; Qian, Y. Q.; Zhang, H. R.; Gao, H. K.; Zhang, L. F.; Zhang, X. X. Superhydrophilic and underwater superoleophobic poly (acrylonitrile-co-methyl acrylate) membrane for highly efficient separation of oil-in-water emulsions. *J. Membr. Sci.* **2018,** *564,* 712-721.

(45) Chaudhary, J. P.; Vadodariya, N.; Nataraj, S. K.; Meena, R. Chitosan-based aerogel membrane for robust oil-in-water emulsion separation. *Acs Appl. Mater. Interfaces* **2015,** *7,* 24957-24962.

(46) Rizzo, C.; Andrews, J. L.; Steed, J. W.; D'Anna, F. Carbohydrate-supramolecular gels: adsorbents for chromium(VI) removal from wastewater. *J. Colloid Interface Sci.* **2019,** *548,* 184-196.

(47) Wang, J.; Gao, M. L.; Shen, T.; Yu, M. M.; Xiang, Y.; Liu, J. Insights into the efficient adsorption of rhodamine B on tunable organo-vermiculites. *J. Hazard. Mater.* **2019,** *366,* 501-511.

(48) Thakur, S.; Pandey, S.; Arotiba, O. A. Development of a sodium alginate-based organic/inorganic superabsorbent composite hydrogel for adsorption of

methylene blue. *Carbohyd. Poly.* **2016,** *153,* 34-46.

(49) Jv, X. J.; Zhao, X. W.; Ge, H. C.; Sun, J. Y.; Li, H.; Wang, Q. S.; Lu, H. G. Fabrication of a magnetic poly(aspartic acid)-poly(acrylic acid) hydrogel: application for the adsorptive removal of organic dyes from aqueous solution. *J. Chem. Eng. Data* **2019,** *64,* 1228-1236.

(50) Wen, X.; Yan, C. J.; Sun, N.; Luo, T. T.; Zhou, S. L.; Luo, W. J. A biomass cationic adsorbent prepared from corn stalk: low-cost material and high adsorption capacity. *J. Polym. Environ.* **2018,** *26,* 1642-1651.

(51) Makhado, E.; Pandey, S.; Nomngongo, P. N.; Ramontja, J. Preparation and characterization of xanthan gum-cl-poly(acrylic acid)/o-MWCNTs hydrogel nanocomposite as highly effective re-usable adsorbent for removal of methylene blue from aqueous solutions. *J. Colloid Interface Sci.* **2018,** *513,* 700-714.

(52) Zhang, M. Y.; Song, L. H.; Jiang, H. F.; Li, S.; Shao, Y. F.; Yang, J. Q.; Li, J. F. Biomass based hydrogel as an adsorbent for the fast removal of heavy metal ions from aqueous solutions. *J. Mater. Chem. A* **2017,** *5,* 3434-3446.

(53) Guan, X. Y.; Chang, J. M.; Chen, Y.; Fan, H. J. A magnetically-separable Fe_3O_4 nanoparticle surface grafted with polyacrylic acid for chromium(III) removal from tannery effluents. *Rsc Advances* **2015,** *5,* 50126-50136.

(54) Tang, P. X.; Sun, Q. M.; Zhao, L. D.; Tang, Y. L.; Liu, Y. Q.; Pu, H. Y.; Gan, N.; Liu, Y. Y.; Li, H. A simple and green method to construct cyclodextrin polymer for the effective and simultaneous estrogen pollutant and metal removal. *Chem. Eng. J.* **2019,** *366,* 598-607.

(55) Moharram, M. A.; Allam, M. A. Study of the interaction of poly(acrylic acid) and poly(acrylic acid-poly acrylamide) complex with bone powders and hydroxyapatite by using TGA and DSC. *J. Appl. Polym. Sci.* **2007,** *105,* 3220-3227.

Table of Contents